Journal of Materials Chemistry C

ROYAL SOCIETY OF CHEMISTRY

PAPER

View Article Online
View Journal



Cite this: DOI: 10.1039/d6tc00974c

# Laser-tunable Raman markers based on glass–ceramic/β-carotene mixtures for advanced anti-counterfeiting applications

Alberto Moure, [a] Pablo Rabasco, [ab] Esther Gómez, [c] Vicente García-Juez, [c] José Francisco Fernández [a] and María Fernández-Álvarez *[a]

Received 25th March 2026,
Accepted 3rd May 2026

DOI: 10.1039/d6tc00974c

rsc.li/materials-c

The need for more reliable authentication methods is rapidly increasing due to the significant economic, social, and security losses caused by the counterfeiting of valuable products. This work explores the possibility of using customizable Raman markers from hierarchical mixtures of feldspar glass–ceramic and β-carotene. The detection signal is based on the combination of Raman spectra of inorganic particles and modifiable Raman spectra of the organic compound by isomerization under laser heating. In this work, the preparation of these Raman markers and the β-carotene isomerization conditions have been established. The laser thermal treatment allows obtaining Raman response distributions in which the altered and unaltered regions can be clearly identified by their differences in the Pearson correlation coefficient. These differences can be used to build the encoding of the response for authentication purposes. Thus, a dual modulation of the Raman response can be obtained: spectral modulation, by adjusting the composition, and spatial modulation, by selectively transforming β-carotene in submillimeter regions, making it possible to create custom patterns in a scalable encoding capacity number of unique encodings for each application.



## 1. Introduction

Product counterfeiting represents a growing threat to security, the economy, and consumer confidence in sectors as diverse as pharmaceuticals, electronics, fashion, and currency, representing approximately 3.3% of international trade.[1–3] Protecting these types of products requires increasingly sophisticated strategies capable of anticipating fraud. Therefore, as counterfeiters increasingly refine their methods, security technologies must constantly evolve to stay ahead.[4–9]

Among the different strategies designed to combat counterfeiting, a variety of approaches are encompassed: optically variable inks, fluorescent fibers, coded nanoparticles, or holographic elements that generate complex visual effects,[10–19] most of them to be detected by spectroscopic techniques. Therefore, advances in spectroscopy-based security systems have become particularly effective tools, allowing the creation of unique optical signatures and their verification using complementary analytical methods. In particular, Raman spectroscopy stands out for not requiring sample preparation, being a non-destructive, versatile and easy-to-apply technique, and for offering unique and highly specific spectral signatures, making it a practical alternative for both routine authenticity verification controls and for forensic analysis.[20–26]

Therefore, Raman markers are currently emerging as an efficient solution for advanced authentication, thanks to their ability to generate unique spectral signals through controlled variations in parameters such as the number of bands, shifts, intensities, or relationships between them.[25,27–29] These materials are typically based on non-destructive compounds with a high cross-section, allowing detection even at low concentrations. This characteristic favors the use of low doses in various incorporation vehicles, such as inks, coatings, or polymer matrices, maintaining the efficiency of the Raman marker without compromising the properties of the support. Furthermore, their low cost and versatility make them an attractive option for large-scale security applications.

Recently, new Raman markers have been developed that meet these requirements. They are based on inorganic compounds obtained from mixtures that generate a glassy Si–O–Al matrix and feldspar-like nanocrystallizations[27,28] by reactions with alkaline and alkaline earth elements (Na, K, Ca). These materials, described in a European patent,[28] exhibit a particularly intense Raman signal in the 1000–2000 $cm^{-1}$ region,

[a] Instituto de Cerámica y Vidrio (ICV), CSIC, Kelsen 5, 28049, Madrid, Spain. E-mail: maria.fernandez@icv.csic.es
[b] Escuela de Doctorado UAM, Francisco Tomás y Valiente 2, 28049 Madrid, Spain
[c] Burgos Paper Mill, Fábrica de Moneda y Timbre – Real Casa de la Moneda (FNMT-RCM), Av. Costa Rica 2, 0900, Burgos, Spain

attributed to photoinduced Raman/luminescence processes under 785 nm laser excitation.[30,31] Thanks to these properties, they can be easily incorporated into various substrates, such as paper or functional coatings, offering a stable, versatile, and easy-to-read authentication system.[27]

Furthermore, it is worth noting that authentication systems based on Raman markers aim not only to detect characteristic Raman bands but also to comparatively analyze their relative intensities. Although different formulations of these markers can generate Raman spectra with the same Raman band positions, variations in the intensity ratios constitute a distinctive spectral pattern that functions as an identification code.[27]

Based on these concepts, this work aims to develop a new generation of customizable Raman markers that allow dual modulation, which provides an additional level of security and can be specifically designed for different counterfeit applications.[32] These Raman markers will integrate combined Raman signals from individual compounds, which can also be modified in selected regions thanks to thermal treatment induced by the Raman laser. For that, in this study, the combination of the previously described inorganic feldspar Raman marker[28] with an organic material such as β-carotene is proposed as a customizable Raman marker. β-Carotene, in addition to being a widely studied natural pigment, exhibits intense Raman bands in the visible region, facilitating its detection even at low concentrations.[33,34] In this work, the combination with glass–ceramic particles will allow the system's spectral response to be modulated, generating codable combinations by laser treatment that act as an optical ''fingerprint''. This approach represents a significant advance over single-marker systems, introducing an external modulation that customizes the design of anti-counterfeiting codes. Through controlled spatial distribution, unique spectral patterns can be created, analogous to constructing a QR code but with a codification in the spectral domain. This concept is inspired by QR-based approaches reported in traceability applications, where spatial patterns are used as information carriers, but in the present case, the information is encoded spectrally rather than visually.[35] This procedure facilitates the individual customization of each marker and multiplies the available code numbers and for that, this increased signal complexity significantly hampers reproduction by counterfeiters and expands the applications of Raman spectroscopy in authentication and traceability.

## 2. Experimental procedure

### 2.1. Materials

Customizable Raman markers combine an inorganic Raman marker (designated as RM), consisting of feldspar nanocrystals embedded in a glassy matrix, with an organic material, β-carotene. The RM particles consist of an albite-type glass–ceramic,[28] which shows a strong signal in the Raman shift range from 1000 to 2500 $cm^{-1}$ when excited at 785 nm. To prepare this Raman marker, a 10/90 wt% mixture of kaolin and frit is used, with the following oxide composition: 51.63% $SiO_2$, 8.05% SrO, 2.68% $Na_2O$, 1.46% $K_2O$, 21.14% $Al_2O_3$, 1.10% ZnO, 10.47% CaO, and 3.48% minor oxides. In addition, $TiO_2$ anatase was added to the marker formulation to increase the opacity of the RM due to its refractive index.[36] The mixture is milled in a porcelain jar with alumina balls (1–2 cm diameter) together with 10 wt% of $TiO_2$ anatase powder in water, and then the suspension is sieved through a 63 μm mesh. The powders are dried in an oven at 80 °C for 6 h and sieved again through a 100 μm mesh. They are then thermally treated at 1100 °C for 1 h, with a heating and cooling rate of 5 °C $min^{-1}$. After thermal treatment, the Raman marker undergoes ball milling again and is dried to produce a powder material.

A source of β-carotene-derived pigment was supplied from the company Flavorix (Spain) in the form of a commercial food-grade coloring powder containing 10% β-carotene, with the remaining components consisting of modified starch, starch, corn oil, α-tocopherol, and ascorbic acid, according to the manufacturer's technical sheet. The particle size distribution was measured using laser diffraction (Malvern Mastersizer S, 632.8 nm He–Ne laser) after ultrasonic dispersion of the powder in an ethanol suspension. In this work, customizable Raman marker mixtures were prepared with the RM marker and β-carotene in different proportions by weight: 95/5, 90/10 and 80/20, respectively, seeking an optimal ratio that allows defining the characteristic Raman bands of each component of the mixture with comparable Raman intensities. In all cases, the mixtures were prepared using a MixerMill 8000D milling system (Spex, USA) for 10 min.

The morphology of the raw powders (RM and β-carotene) and the mixtures was analyzed using a field-emission scanning electron microscope (FE-SEM), employing a Hitachi S-4700 (Japan) operated at 20 kV.

Thermogravimetric analysis using a TA Q50 (TA Instruments, USA) was performed to observe differences in thermal behavior of the materials, cycling from 25 to 600 °C, at 10 °C $min^{-1}$ and using an air/argon atmosphere.

### 2.2. Customization of markers with laser treatment

For the customization of the Raman markers, a laser treatment was performed for each mixture composition, adapting the laser power for each one. Thanks to the focused laser, it was possible to perform selective spatial treatment in the regions where the laser was applied at the optimal power for this purpose. To have local heating necessary for the customization, a susceptor (carbon black, CB) is added to the initial mixture. The CB used was PUREX HS 55 powder, provided by Degussa (Germany), which is characterized by a density of 0.335 g $cm^{-3}$, a high specific surface area of 40 $m^2$ $g^{-1}$, and an agglomerate size between 1.4 and 1.7 μm. The full particle size distribution can be found in the supplementary information (SI), Fig. S1. This resulted in areas within the samples that were treated and untreated with the laser. A representative scheme of the process is shown in Fig. 1.

### 2.3. Demonstrator preparation with customizable markers

A polymeric support was chosen as the vehicle to integrate the customizable Raman markers into a medium that simulates

 


Fig. 1 Scheme of the marker mix customization process.

their practical application and can be easily attached to the object intended for anti-counterfeiting protection. For this purpose, a transparent epoxy matrix has been chosen to act as a fixing element for the powder markers. A RM/β-carotene (80/20 wt%) mixture with a 5 wt% of CB added was dispersed in the epoxy with a weight ratio of epoxy/powder of 80/20. The dispersions were made using a commercial two-component transparent epoxy TRANSLUX D 150 (Feroca, Madrid), which is highly resistant to ultraviolet light. To ensure good distribution of the marker powders in the epoxy, a mixture containing the two components of the epoxy resin (in a 2 : 1 weight ratio) was first homogenized with the marker powder mix using a laboratory mixer model DSV.SL-1 (LLEAL, S.A.) for 2 min at 2700 rpm. The obtained material was poured into plastic molds and left to cure at 40 °C for 48 h.

### 2.4. Raman spectroscopy characterization

Raman spectroscopy was performed using a portable B&W Tek iRaman spectrometer (B&W Tek, USA) with a 785 nm laser (290 mW as maximum power) and a 20× objective lens. The laser measurement spot size is approximately 100 μm in diameter. The measurement conditions (laser power and integration time) were different for each mixture in order to optimize the Raman measurements in each case, so they are specified throughout the manuscript, as well as in a summary table in the SI (Table S1). Raman spectra at increasing temperatures were acquired by coupling a Linkam THMS600 thermal chamber (Linkam, UK) to the B&W Tek iRaman spectrometer.

Furthermore, all laser treatments performed for this work were carried out using the Raman spectrometer's own laser.

## 3. Results and discussion

Customizable markers were created by mixing the RM and the organic component β-carotene. The RM was selected for this study because it exhibits high intensity Raman bands between 1000 and 2000 $cm^{-1}$.[28] Furthermore, this RM exhibits a number of other Raman spectral characteristics. On the one hand, Raman bands characteristic of rutile are observed (~143, 447 and 612 $cm^{-1}$), indicating that the $TiO_2$ added during fabrication underwent a phase transformation from anatase to rutile during heat treatment.[37] Additionally, Raman bands associated with other low-intensity photoinduced Raman/luminescence processes in RM are also detected at Raman shifts below 1000 $cm^{-1}$ [38,39] in coexistence with the pure rutile Raman bands. Besides, β-carotene is a natural dye that exhibits a Raman spectrum with two narrow and high-intensity Raman bands located at 1156 and 1518 $cm^{-1}$, which are, in principle, compatible with those of the RM, as shown in Fig. 2a. These Raman bands are related to the carbon–carbon double bond (C═C) and single bond (C–C) stretching vibrations of the polyene chain, respectively.[40] Thus, the combined Raman response of RM and β-carotene should provide a new family of Raman markers characterized by Raman spectra with multiple bands that are ideal for anti-counterfeiting applications.

The particle size distribution of β-carotene and RM is shown in Fig. 2b and c, respectively. In the case of β-carotene, it comprises three distributions, centered approximately at 0.8, 15 and 300 μm. The D50 size of the whole particle distribution was 222 μm. In contrast, RM sizes show a bimodal distribution, centered at approximately 2 and 9 μm, with a tail of bigger particles, probably agglomerates with mean sizes close to 80 μm. In this case, the D50 size of the whole particle distribution was 5.6 μm. Despite the apparently inappropriate characteristics of the β-carotene precursor powder used (low content and high particle size), it gave the correct behavior for the purpose of this work, as will be shown in the manuscript, but with a very noticeable reduction of the price (109.5 € $kg^{-1}$) with respect to highly pure β-carotene (21.400 € $kg^{-1}$).

Mixtures of the RM with β-carotene were prepared at different weight ratios: 95/5, 90/10 and 80/20, seeking an optimal ratio that would allow defining the characteristic Raman bands of each component of the mixture with comparable Raman intensities. The accuracy of the proportions between both materials was checked by thermogravimetric measurements (shown in Fig. 2d for the 80/20 mixture, as representative). Besides, this study shows three major weight losses for β-carotene, associated with increasing temperature to the desorption of residual moisture (at $T < 150$ °C); the onset of a thermal degradation (at 260 °C, approximately) with losses of small parts of the β-carotene chains; and a main decomposition of the whole structure, triggered at 350 °C.

Fig. 3a and b show the SEM images acquired for the β-carotene and the RM, respectively. The particles of the

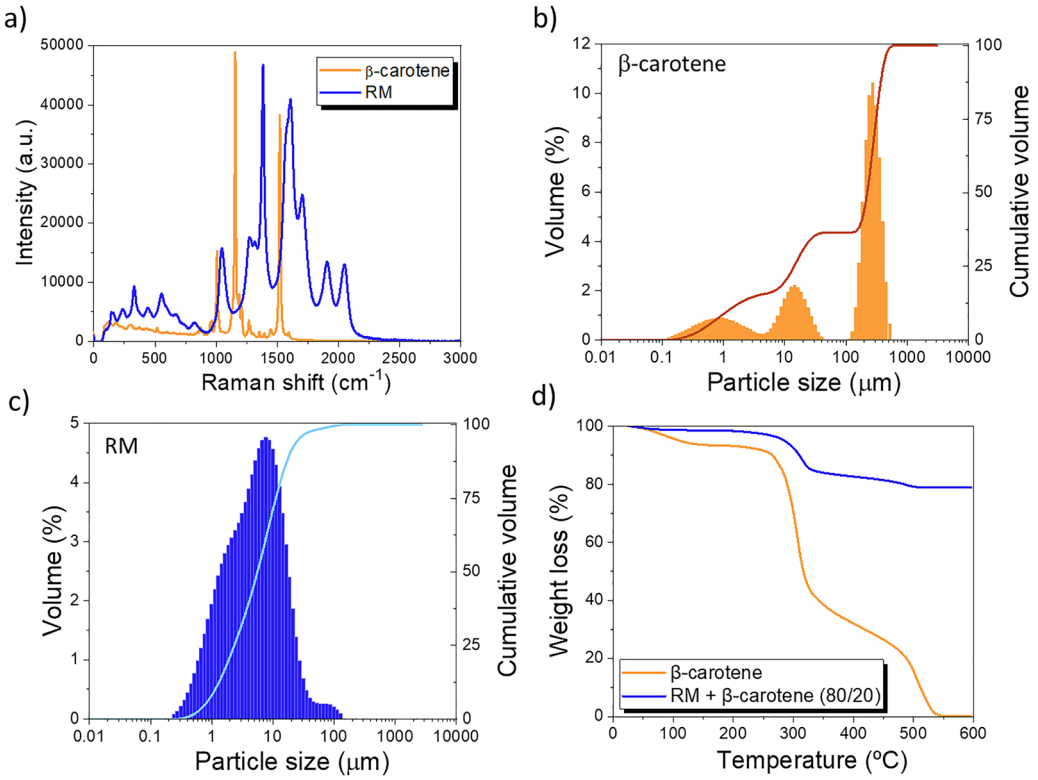


Fig. 2 (a) Representative Raman spectra of the β-carotene and RM materials used for the fabrication of the customizable marker; (b) and (c) particle size distributions of the β-carotene and RM; (d) thermogravimetric curve of β-carotene and the mixture RM/β-carotene with a weight ratio of 80/20.

commercial precursor of β-carotene used in this work consist of submicrometric spherical granules with β-carotene distributed on their surface, while the particles corresponding to RM have smaller sizes and flat surfaces, as corresponds to its glass–ceramic nature. The mixtures of both materials are built with hierarchical microstructures,[41] as shown in Fig. 3, where the β-carotene with sizes in the range of 0.5–1 μm envelops the larger micrometric RM particles. First, the preparation of the mixtures did not induce any detectable alteration in the initial morphology of the RM particles (Fig. 3). It seems that during the mixing step, there is also a milling process where the large particles of the β-carotene precursors are mechanically ground, allowing the transformation to smaller particles that distribute on the surface of the RM material. Besides, the mixing process promotes the adhesion of β-carotene to the RM surface. The image reveals that as the β-carotene content increases, a greater

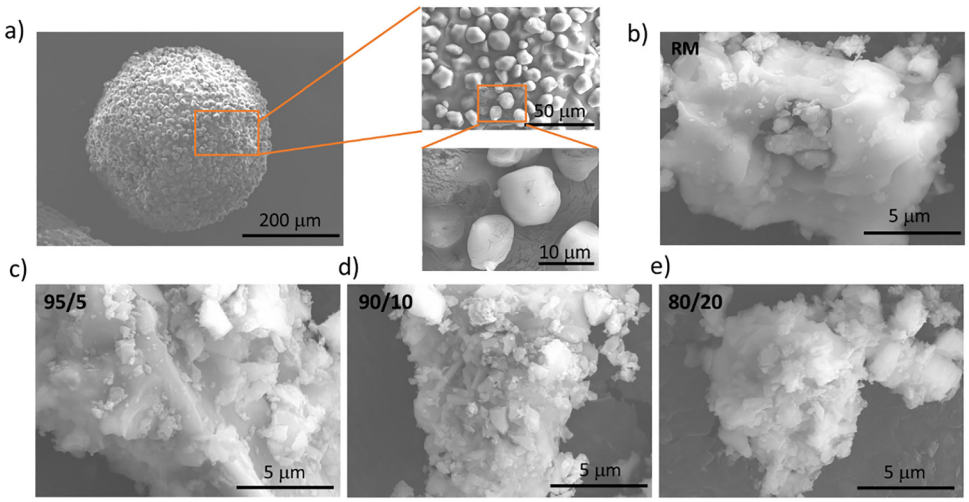


Fig. 3 SEM images of the particles of: (a) β-carotene; (b) Raman marker (RM) and the mixtures RM/β-carotene with weight ratios of (c) 95/5; (d) 90/10 and (e) 80/20.

portion of the Raman marker's surface becomes coated with β-carotene. In addition, this hierarchical particle distribution is important because it ensures that both the RM and β-carotene are simultaneously illuminated by the laser used for characterization (laser spot ~100 μm).

Following the morphological study, the Raman responses of the different mixtures were analyzed. Fig. 4a shows the entire and the magnified Raman spectra of the mixtures with different relative amounts of RM and β-carotene. They show how the Raman bands of each component are combined. The magnified Raman spectra comparing the different proportions of RM/β-carotene in the mixture show that the Raman main bands located at 1156 and 1518 $cm^{-1}$ increase in intensity relative to those of the RM as the amount of pigment increases. This fact opens the possibilities of considering each new mixture as a single security Raman marker. The fact that each composition exhibits a different spectral signature is relevant to the fight against counterfeiting, as it allows for the creation of multiple identifiable signatures from the same raw materials. These spectral differences are what allow the modulation of different customizable Raman markers.

To estimate the ability to differentiate between the Raman signals, the Pearson correlation coefficients (PC) (eqn (1)) of the Raman spectra for the 90/10 and 80/20 mixtures were calculated with respect to the 95/5 composition. PC values can range from 0 to 1, where values closer to 1 indicate a high correlation between spectra (*i.e.*, greater similarity between Raman spectra). In this case, the 95/5 composition has a correlation factor equal to 1 because it was taken as the reference. A decrease in PC values is associated with greater differences between spectra, meaning that lower PC values indicate a higher capacity to discriminate signals during the authentication process of the corresponding valuable object. The following equation was used for the calculations:

$$PC = \frac{\sum_{i=1}^{n}(X_i - \bar{X})(Y_i - \bar{Y})}{\sqrt{\sum_{i=1}^{n}(X_i - \bar{X})^2}\sqrt{\sum_{i=1}^{n}(Y_i - \bar{Y})^2}} \quad (1)$$

where $X_i$ and $Y_i$ are the individual values of the Raman shift and intensity at each point of the spectra, respectively, $\bar{X}$ and $\bar{Y}$ are their mean values, and $n$ is the number of points within each Raman spectrum. The calculation was carried out for the derivatives of each Raman spectrum in order to highlight local changes in the Raman spectra. The correlation factor decreases as the β-carotene content increases, having values lower than 0.9 for the 80/20 mixture. The major differences that lead to a decrease in the PC values come from the increasing intensity ratios of the Raman bands at 1156 $cm^{-1}$ (from the β-carotene) and 1382 $cm^{-1}$ (from the RM). This means that mixtures with different proportions result in markers with the

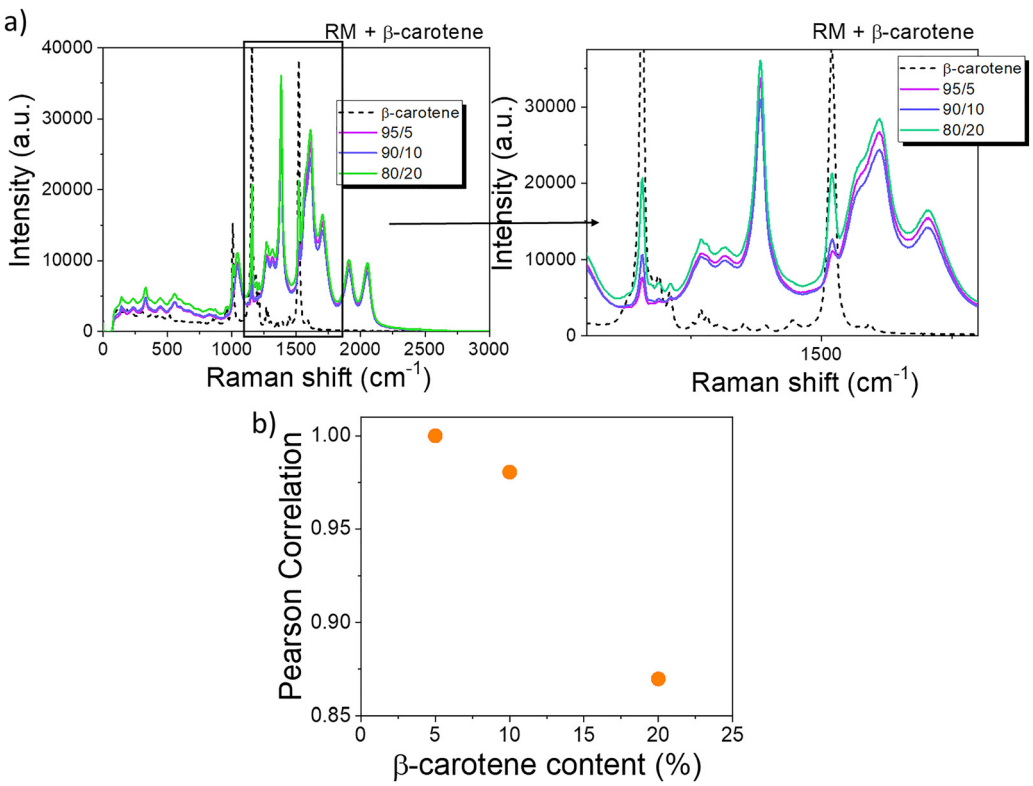


Fig. 4 (a) Complete Raman spectra and magnification between 1050 and 1800 $cm^{-1}$ of different powder RM/β-carotene mixtures with various percentages and intensity ratio variations. (b) Pearson correlation factor for the ratios RM/β-carotene content of 90/10 and 80/20 compared to 95/5 (which takes a value of 1) in the mixtures.

same Raman bands but varying relative intensities, allowing them to be considered as different markers for authentication purposes.

The concept of customizable markers is based on the capability of modifying the Raman spectrum of a mixture in a selected spatial region by inducing a change in its response driven by high-power laser illumination. In the mixtures of this work, this change will be due to β-carotene isomerization. According to the literature, a local temperature of approximately 60 °C can initiate this process,[42] which is accelerated at temperatures higher than 100 °C,[43] leading consequently to the modification of the β-carotene Raman spectrum. These conditions cannot be achieved in mixtures of RM and β-carotene alone, as the required isomerization is not reached even under the maximum available laser power (290 mW). Consequently, no differences were observed in the Raman spectra after the laser treatments.

To achieve the conditions required for the transformation of β-carotene, the same mixtures were prepared with the addition of 5 wt% carbon black (CB). This material acts as a susceptor, absorbing part of the laser irradiation and generating localized heating, which in turn promotes β-carotene isomerization and modifies the Raman spectrum of the mixtures. In addition, it is worth noting that CB bands are not distinguishable in these Raman spectra because they have a much smaller cross-section compared to RM and the β-carotene.

The study of the transformation of the Raman spectra of β-carotene/RM mixtures was carried out using the 80/20 composition with the addition of 5 wt% CB as a susceptor, as shown in Fig. 5. In the measurement protocol, the Raman spectra of the RM marker/β-carotene mixture were first recorded at a laser power of 6 mW using the 785 nm wavelength laser (referred to as the initial). Subsequently, the sample was exposed to laser powers of 17 mW and 31 mW (in the process referred to as "laser treatment"). These were the laser powers at which β-carotene isomerization was triggered without degradation, so they were chosen for the treatment. After this, they were then re-measured at 6 mW. The complete Raman spectra obtained, covering Raman shifts from 0 to 3000 $cm^{-1}$, together with magnified views of the 1050 and 1800 $cm^{-1}$ region, are shown in Fig. 5a. In this graph, it can be observed that the characteristic Raman bands of β-carotene (located at 1156 and 1518 $cm^{-1}$) disappear or decrease in Raman intensity after the laser treatment. A slight increase in fluorescence is also observed, although it does not prevent the Raman signal from being detectable.

The change in the Raman spectra before and after laser treatment due to the decrease in the Raman intensity of the β-carotene Raman bands was monitored again using the Pearson Correlation factor applied to the derived Raman spectra curves. It was plotted at different burning power levels and the graph is shown in Fig. 5b. A constant decrease in the PC factor

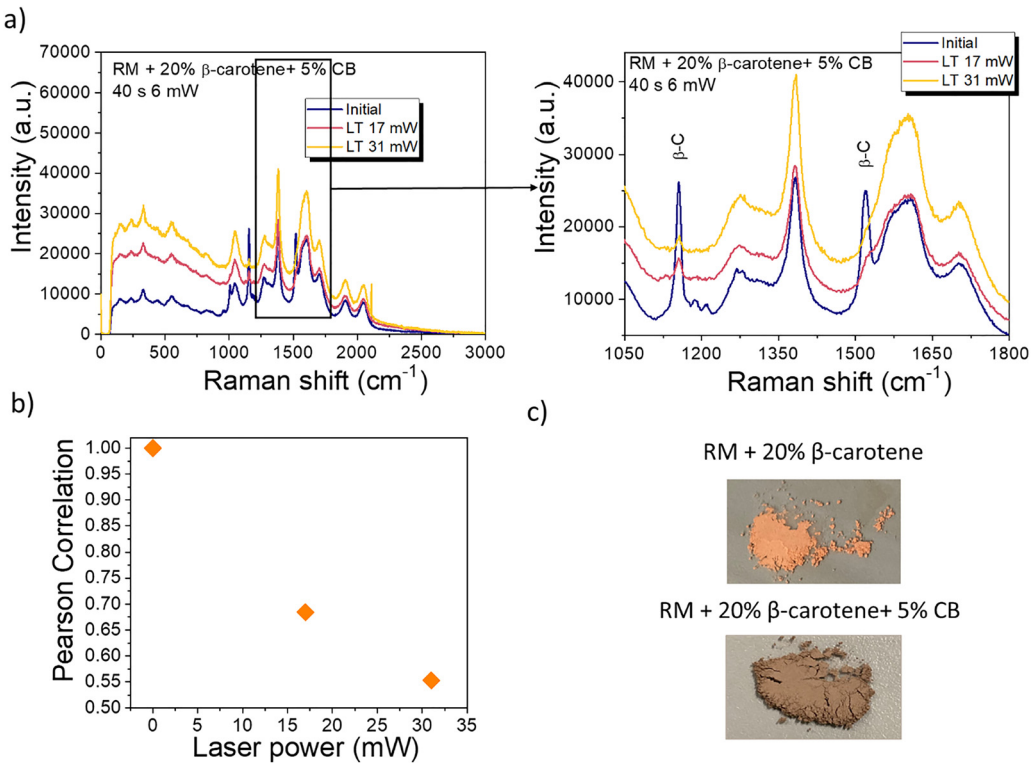


Fig. 5 Raman signal variations of an RM/β-carotene mixture with an 80/20 weight ratio and 5 wt% CB as a susceptor. (a) Complete Raman spectra and magnification between 1050 and 1800 $cm^{-1}$ at different laser powers. (b) Pearson correlation factor of the Raman spectra as a function of the laser powers, compared to that before laser treatment (Pearson coefficient = 1). (c) Characteristic color of a mixture of the RM with β-carotene in a weight ratio of 80/20 and the same mixture with a 5 wt% of CB.

is observed, caused by the laser treatment, with values lower than 0.7 after β-carotene degradation under the two laser powers tested. Thus, the Raman spectra of unmodified and modified regions are perfectly distinguishable, which is essential for the final application. With these results, spectral modulation within customizable markers is possible.

In addition, Fig. 5c shows photographs of the powders corresponding to the different mixtures. The RM mixture containing β-carotene exhibits an orange coloration, as expected from the use of this red dye. However, once CB is added, the resulting mixture becomes noticeably darker, acquiring a browner tone.

The modification of the Raman spectra is associated with the isomerization of β-carotene,[44] which is favored by the presence of the C=C double bonds,[43] in a process where the major and more stable all-*trans*-β-carotene species transform into several *cis*-β-carotene species.[44] The isomerization leads to a change in the Raman spectra, as the bond's polarizability decreases by the change in the electronic configuration induced by the presence of the *cis* species,[45] particularly those corresponding to C=C bands. This results in a decrease in their Raman intensity. Thus, the temperature reached during the laser treatment can be monitored using the intensity ratio of the main Raman bands located at 1156 and 1518 $cm^{-1}$.

To experimentally verify the spectral modifications associated with the isomerization of β-carotene and the resulting changes in the relative Raman band intensities described above, temperature experiments were carried out. Fig. 6a and b show the Raman spectra of β-carotene and the RM/β-carotene mixture, respectively, measured at different temperatures, together with magnified views of the spectral range where the main Raman bands of β-carotene appear. Changes in the intensity and Raman shift are observed. Raman shift positions of the main β-carotene bands are affected by temperature, as shown in Fig. S2, due to the expansion of the bonds and the change in polarizability during isomerization. A red shift (expansion) is more noticeable for the band located at 1156 $cm^{-1}$, while the band located at 1518 $cm^{-1}$ is more affected by isomerization, showing a significant blue-shift during this process. A clear evolution of the Raman bands with increasing temperature is also observed, with a continuous reduction of their Raman intensity, which becomes highly pronounced from 175 °C to 200 °C in the case of the measurement for β-carotene. The Raman intensity ratios between the intensities of the Raman bands of β-carotene located at 1156 and 1518 $cm^{-1}$ were calculated up to 250 °C from the Raman spectra. Their values are shown in Fig. 6c for pure β-carotene and for the mixture with RM. It must be taken into account that the β-carotene Raman band located at 1518 $cm^{-1}$ coincides with one of the characteristic Raman bands corresponding to the RM, so the Raman intensity measured for this Raman band in the mixtures corresponds to the sum of both contributions that cannot be separated. This explains why the values are different when comparing the ratios calculated with the mixtures and only in β-carotene. This fact adds greater uncertainty in their measurements, reflected in the higher values in the error bars. In any case, the isomerization is an irreversible process, evidenced by the variation in the intensity ratios. From the values calculated for the mixture after laser treatment from the graphs shown in Fig. 5a and the linear interpolation of the ratios data shown in Fig. 6c, an estimation of the temperature reached in the laser treatment of the β-carotene/RM mixtures can be obtained. Considering that the intensity ratio is 0.76 for a power of 17 mW and 0.55 for 31 mW, and applying error propagation analysis to estimate the uncertainty in the temperature estimated, the results show that the calculated temperature reached at 17 mW is 245 ± 1 °C, while at 31 mW it is 268 ± 4 °C. It is important to note that the reported temperatures should be understood as approximate values specific to this system, used to identify the onset of β-carotene isomerization below the temperatures where β-carotene begins to volatize, as the thermogravimetric study shows (Fig. 2d), and not as precise absolute temperature measurements.

The typical discoloration of β-carotene appearing during the isomerization process[46,47] was observed and was taken as additional evidence of the process observed during marker customization. Fig. 7a shows the initial white/beige color of the RM, while Fig. 7b shows the color evolution of the customizable marker under laser irradiation. Initially, the compacted RM exhibits a whitish color associated with the RM mixed with very small particles of β-carotene and CB. In addition, orange particles attributed to agglomerated β-carotene and black particles corresponding to agglomerated CB can also be observed. After the laser irradiation, a noticeable color change is observed in the customizable marker. When a laser power of 17 mW is applied, a change in the surface color occurs, turning blue in the center of the laser print and yellowish in the crown, the print being more pronounced when burning at 31 mW. The center appears blue because the laser beam concentrates its highest power there, producing stronger heating and thus complete isomerization of β-carotene, while the surrounding yellow ring corresponds to areas that were heated less and therefore underwent only partial isomerization. The higher the laser power, the larger the bleached area becomes. Besides, the CB particles appear to increase in size during irradiation, which is interpreted as a localized burning effect induced by the laser treatment. For this same reason, the orange color of certain clusters of β-carotene is no longer visible after the laser treatment.

In the application, the Raman marker must be incorporated into a matrix in order to provide a fixing element for the customizable marker, while also serving as a protective medium in which the Raman marker can be embedded to ensure stability and durability. The vehicle employed was an ultraviolet-resistant epoxy resin that helps prevent β-carotene oxidation, which triggers its natural degradation, in addition to being the fixing element. The same RM + β-carotene 80/20 + 5% CB mixture was further dispersed in epoxy at 20 wt%, and laser treatment similar to that conducted on the powder mixtures was performed. This phenomenon is reflected in the Raman spectra as shown in Fig. 8a. The initial measurement carried out with a laser power of 17 mW and an integration time of 10 s

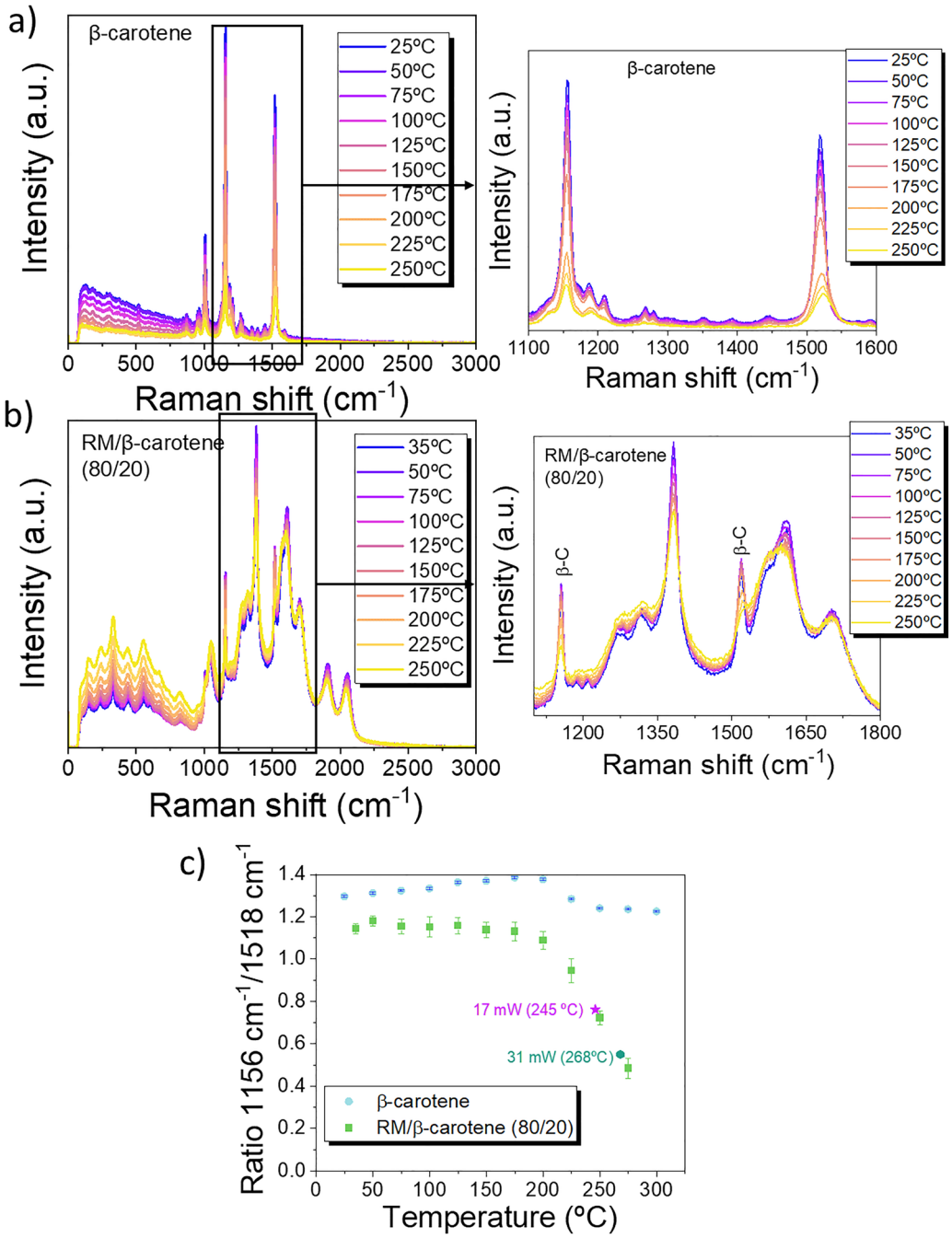


Fig. 6 Raman spectra of (a) β-carotene and (b) RM/β-carotene mixture as a function of temperature; (c) intensity ratio of the β-carotene Raman bands located at 1156 and 1518 $cm^{-1}$ for isolated β-carotene and for the RM/β-carotene mixture and the estimation of the temperature reached in the RM/β-carotene mixture after the laser treatments at 17 and 31 mW (245 and 268 °C, respectively) obtained from the extrapolation of the values in the RM/β-carotene mixture curve.

clearly shows the coexistence of the Raman bands corresponding to β-carotene and the Raman marker. As can be seen, the epoxy Raman bands are not visible due to their low intensity compared to the other bands of RM and β-carotene (Fig. S3). After the laser treatment with a power of 45 mW during 10 s in order to carry out isomerization, the Raman spectrum (Fig. 8a) measured under the same initial conditions (17 mW and 10 s) reflects the decrease in the intensity of Raman β-carotene bands. This phenomenon is even greater when the laser power is increased to 54 mW. Similarly, to the study in powder form, the temperature reached in the process can be estimated from the intensity ratio of the main β-carotene Raman bands located at 1156 and 1518 $cm^{-1}$. The values calculated were 1.05 and 0.98 after laser treatment at 45 and 54 mW, respectively. The equivalent temperatures according to the curve shown in Fig. 6 are estimated as 207 and

 

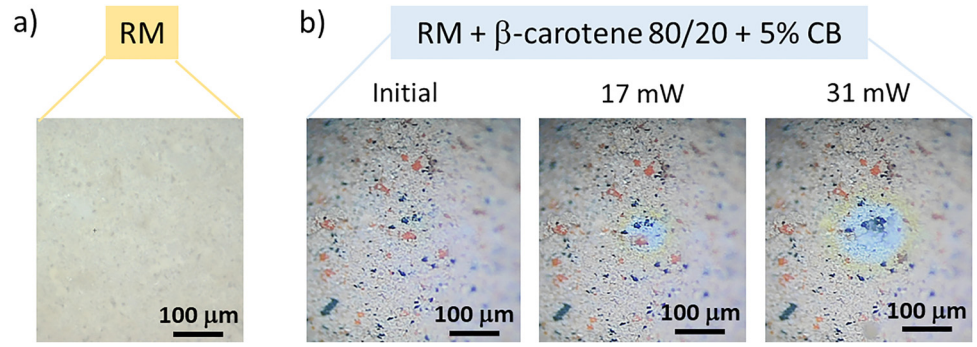


Fig. 7 (a) Microscopic image of RM and (b) microscopic evidence of β-carotene volatilization by laser action in the RM + β-carotene 80/20 + 5% CB powder.

220 °C. Once again, these temperatures must be taken as indicative of those reached in the process, which in any case are above the temperature where isomerization takes place. It should be noted that in the samples with epoxy resin, higher laser powers were used (45 and 54 mW instead of 17 and 31 mW) since the epoxy matrix favors heat dissipation, which reduces the local temperature increase under the same irradiation conditions, so a higher laser power is required to achieve a comparable photothermal activation within the material. The changes induced in the Raman spectra are reflected in the Pearson correlation calculated and shown in Fig. 8b, with values lower than 0.9, which are acceptable values to distinguish regions with altered and unaltered Raman signals.

A mechanism of customization for the marker combining RM, β-carotene and CB in a vehicle (epoxy in this case) is proposed in Fig. 9, where the three materials coexist in the epoxy matrix. It should be noted that epoxy is shown in gray to improve the contrast of the image, even though it is transparent. During laser treatment, CB acts as a susceptor absorbing the laser radiation that increases the local temperature. Following laser treatment, while CB and RM particles do not suffer any variation, the isomerization of β-carotene (represented in Fig. 9 by the change to blue) occurs in the areas of laser radiation. This process allows the isomerization of β-carotene in selected regions (shown in blue in Fig. 9) while leaving others unchanged (remaining grey in Fig. 9), allowing the

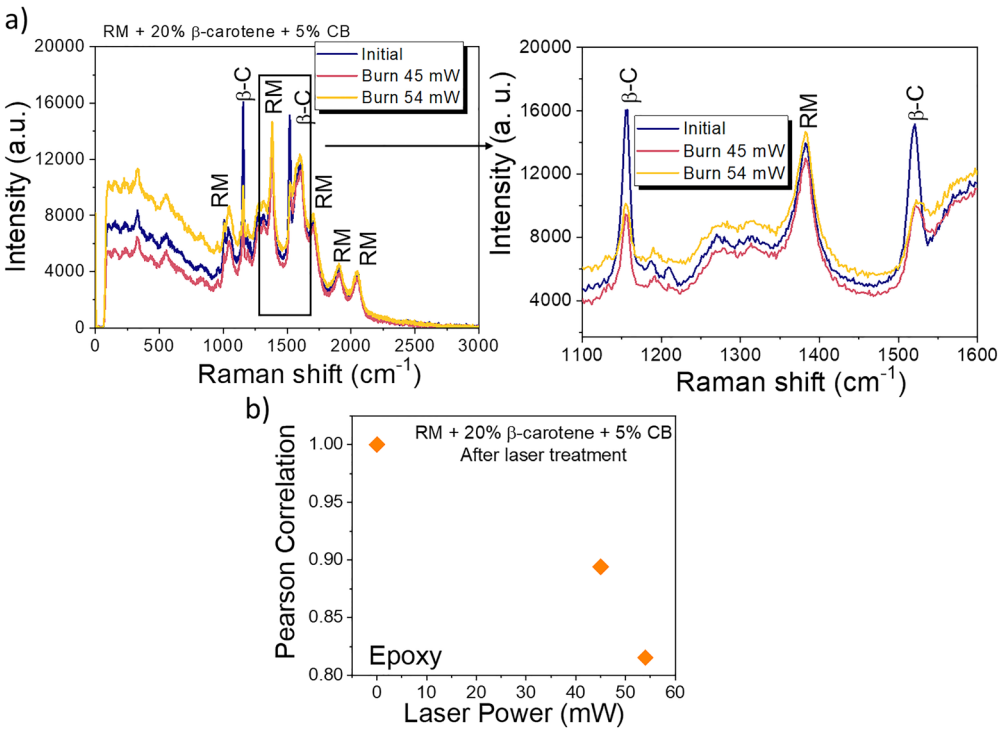


Fig. 8 (a) Complete Raman spectra and magnification between 1050 and 1800 $cm^{-1}$ of RM/β-carotene of an 80/20 weight ratio mixture with 5 wt% as a CB susceptor embedded in an epoxy matrix. (b) Pearson correlation factor of the Raman spectra as a function of the laser powers, compared to that before laser treatment (Pearson coefficient = 1) for the customizable marker embedded in the epoxy vehicle.

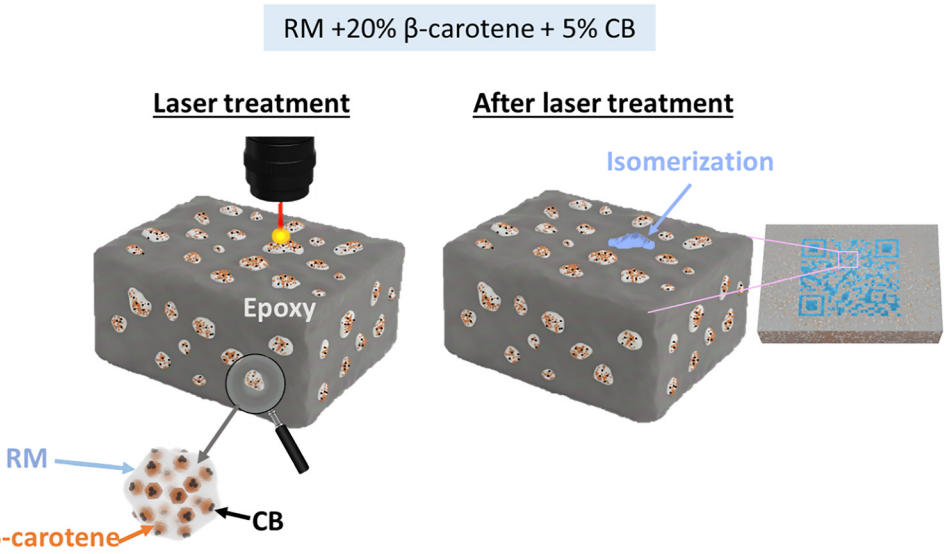


Fig. 9 Mechanism for customizing an RM/β-carotene mixture (80/20 weight ratio) with 5 wt% CB as a susceptor embedded in an epoxy matrix.

creation of QR code-like patterns, as also illustrated in Fig. 9. This pattern could only be revealed by an authentication CRM measurement, in which the Raman spectra in blue areas would correspond to RM and in the grey areas to the combined RM/β-carotene signal.

These results demonstrate the potential of this customizable Raman marker system to generate spatially encoded spectral patterns through laser treatment. The ability to modulate the Raman response through localized controlled isomerization of beta-carotene mixed with inorganic Raman markers allows for the creation of suitable combinations for anti-counterfeiting. Furthermore, by integrating the customizable marker into a stable matrix and activating its spectral transformation in specific desired areas, it is possible to implement invisible yet verifiable signatures that resist counterfeiting. The encoding capacity of this type of system is determined by spatial information, which depends on the physical distribution of the materials within the detection area, and by spectral information, which is related to the differences in the Raman spectra of the species present. In the article by Y. Huo *et al.*,[48] it is established that the encoding capacity ($C$) for a region in which spectroscopic signals can be distinguished is given by the expression (eqn (2)):

$$C = (nm)^p \tag{2}$$

where $p$ is the number of pixels (or measurement points), $m$ is the number of types of molecules or crystalline structures present, and $n$ is the number of detectable variables. In our case, the value of $m$ is 2 (marker and beta-carotene), and the number of detectable variables is also 2 (using an identification factor based on the Pearson correlation coefficient, which determines when modified and unmodified regions can be distinguished).

The number of pixels is determined in part by the size of the laser beam spot. If identification is carried out by confocal Raman microscopy using a 100× objective, the beam size can be calculated from the expression (eqn (3)):

$$d = \frac{1.22\lambda}{\mathrm{NA}} \tag{3}$$

where $\lambda$ is the wavelength and NA is the numerical aperture of the objective. Typical values of approximately 1 μm are obtained for 785 nm lasers with a 100× objective. Therefore, in a 15 × 15 μm image, using a 1.5 μm step size (that is, burning one point and leaving a 0.5 μm margin to prevent overlap between consecutively burned regions), approximately 10 × 10 lines (100 points) would be obtained. The encoding capacity would therefore be: $(2 \times 2)^{100}$, that is, a theoretical encoding capacity on the order of $10^{43}$. This approach offers a versatile new method for the secure marking of objects, adaptable to diverse sectors such as the authentication of high-value products, pharmaceutical traceability, defense applications, and the preservation of cultural heritage.

## 4. Conclusions

This work presents a novel approach to fabricate customizable Raman markers based on the hierarchical mixture of an inorganic feldspar glass–ceramic and organic β-carotene. The mixture became a tunable Raman marker that can be selectively modified by laser-induced isomerization of the β-carotene component. The integration of carbon black as a susceptor enables localized heating, allowing controlled transformation of β-carotene and the generation of spatially encoded Raman patterns. This strategy provides dual modulation of the Raman response: a Raman spectral modulation, through composition tuning and β-carotene isomerization, and spatial modulation, through selective transformation in specific regions. Therefore, the main conclusions of this work are:

• The Raman spectra of the RM/β-carotene mixtures, organized in hierarchical microstructures where β-carotene coats RM particles, can be modulated by adjusting the composition and laser parameters, resulting in distinguishable Raman spectral signatures.

• Laser-induced isomerization of β-carotene produces irreversible changes in its Raman bands, particularly those associated with C=C stretching, which can be monitored using intensity relationships and Pearson correlation analysis. This irreversible transformation enables the generation of unique, non-reproducible spectral codes.

• The incorporation of the new customizable RM/β-carotene + CB markers into polymer matrices demonstrates their viability for practical applications without compromising their tunable Raman response. Following laser irradiation, β-carotene isomerization produces spatially controllable spectral transformation, enabling the generation of laser-encoded patterns that can be authenticated by their Raman signal.

• These customizable markers open new possibilities for anti-counterfeiting applications by combining dual modulation (spectral and spatial), allowing the generation of unique spectral codes tailored to specific applications.

## Conflicts of interest

There are no conflicts to declare.

## Data availability

The data used to support the findings of this study are included within the article and in the supplementary information (SI). Supplementary information is available. See DOI: https://doi.org/10.1039/d6tc00974c.

## Acknowledgements

The authors disclosed the receipt of the following financial support for the research, authorship, and/or publication of this article. This work was supported by the CSIC Project AFICHES (no. 202460E101) and AEI-MICIU PID2023-153398OB-I00.

## References

1 I. Butt, M. K. Al Balushi, S. H. Lee, M. Mohan, N. Ahmad Khan and S. Haines, Four decades of counterfeit research: A bibliometric analysis, *Cogent Bus. Manag.*, 2023, **10**, 2284814, DOI: 10.1080/23311975.2023.2284814.

2 K. Dégardin, Y. Roggo, F. Been and P. Margot, Detection and chemical profiling of medicine counterfeits by Raman spectroscopy and chemometrics, *Anal. Chim. Acta*, 2011, **705**, 334–341, DOI: 10.1016/j.aca.2011.07.043.

3 M. Gué, M. Cegłowski, M. Pawlaczyk, J. Kurczewska, E. Reszke and G. Schroeder, Application of FAPA mass spectrometry for analysis of fragrance ingredients used in cosmetics, *Measurement*, 2021, **168**, 108326, DOI: 10.1016/j.measurement.2020.108326.

4 V. Sharma, R. Chopra, N. Verma, P. K. Mishra and R. Cieśla, Infrared and Raman spectroscopy in conjunction with chemometric methods in questioned document analysis: Forensic applications, *TrAC, Trends Anal. Chem.*, 2024, **180**, 117989, DOI: 10.1016/j.trac.2024.117989.

5 A. Tomar, R. R. Gupta, S. K. Mehta and S. Sharma, An Overview of Security Materials in Banknotes and Analytical Techniques in Detecting Counterfeits, *Crit. Rev. Anal. Chem.*, 2023, 1–14, DOI: 10.1080/10408347.2023.2209185.

6 J. Liu, L. He, D. Li, X. Wang, L. Liu, J. Lin and K. Huang, Developing multi-mode phosphor with non-visible ranges for advanced anti-counterfeiting in medicine, *Mater. Des.*, 2025, **260**, 115023, DOI: 10.1016/j.matdes.2025.115023.

7 X. Dong, P. Wu, C. G. Schaefer, L. Zhang, C. E. Finlayson and C. Wang, Solvatochromism based on structural color: Smart polymer composites for sensing and security, *Mater. Des.*, 2018, **160**, 417–426, DOI: 10.1016/j.matdes.2018.09.026.

8 B. Yoon, J. Lee, I. S. Park, S. Jeon, J. Lee and J. M. Kim, Recent functional material based approaches to prevent and detect counterfeiting, *J. Mater. Chem. C*, 2013, **1**, 2388–2403, DOI: 10.1039/c3tc00818e.

9 Q. Wang, D. Zhou, K. Gong, X. Lv, P. Li and Y. Liu, A multidimensional *anti*-counterfeiting dynamic flexible label based on light/thermal responsive CLC microspheres, *J. Mater. Chem. C*, 2024, **12**, 15092–15100, DOI: 10.1039/d4tc02630f.

10 Y. Liu, F. Han, F. Li, Y. Zhao, M. Chen, Z. Xu, X. Zheng, H. Hu, J. Yao, T. Guo, W. Lin, Y. Zheng, B. You, P. Liu, Y. Li and L. Qian, Inkjet-printed unclonable quantum dot fluorescent *anti*-counterfeiting labels with artificial intelligence authentication, *Nat. Commun.*, 2019, **10**, 1–9, DOI: 10.1038/s41467-019-10406-7.

11 W. Ren, G. Lin, C. Clarke, J. Zhou and D. Jin, Optical Nanomaterials and Enabling Technologies for High-Security-Level Anticounterfeiting, *Adv. Mater.*, 2020, **32**, 1–15, DOI: 10.1002/adma.201901430.

12 A. Abdollahi, H. Roghani-Mamaqani, B. Razavi and M. Salami-Kalajahi, Photoluminescent and chromic nanomaterials for anticounterfeiting technologies: Recent advances and future challenges, *ACS Nano*, 2020, **14**, 14417–14492, DOI: 10.1021/acsnano.0c07289.

13 H. Suo, Q. Zhu, X. Zhang, B. Chen, J. Chen and F. Wang, High-security *anti*-counterfeiting through upconversion luminescence, *Mater. Today Phys.*, 2021, **21**, 100520, DOI: 10.1016/j.mtphys.2021.100520.

14 S. Paikray, S. K. Ray, P. Nayak, A. K. Sahoo, S. N. Prusty, S. Dash and S. S. Nanda, Comparative analysis of $Sm^{3+}$-doped BaWO4 and CaWO4 phosphors: Properties and application in latent fingerprints and *anti*-counterfeiting, *J. Alloys Compd.*, 2025, **1010**, 177666, DOI: 10.1016/j.jallcom.2024.177666.

15 L. Chu, X. Zhang, W. Niu, S. Wu, W. Ma, B. Tang and S. Zhang, Hollow silica opals/cellulose acetate nanocomposite

films with structural colors for *anti*-counterfeiting of banknotes, *J. Mater. Chem. C*, 2019, **7**, 7411–7417, DOI: 10.1039/c9tc01992h.

16 H. Hu, H. Zhong, C. Chen and Q. Chen, Magnetically responsive photonic watermarks on banknotes, *J. Mater. Chem. C*, 2014, **2**, 3695–3702, DOI: 10.1039/c3tc32228a.

17 L. Xu, H. Lei, Z. Li, W. Liu, Y. Li and Y. Yang, Circularly polarized luminescence with large dissymmetry factors based on perovskite and cholesteric liquid crystal polymer network films, *J. Mater. Chem. C*, 2025, **13**, 7544–7549, DOI: 10.1039/d4tc05268d.

18 N. Vahedigharehchopogh, O. Kıbrıslı, E. Erol, M. Çelikbilek Ersundu and A. E. Ersundu, A straightforward approach for high-end *anti*-counterfeiting applications based on NIR laser-driven lanthanide doped luminescent glasses, *J. Mater. Chem. C*, 2021, **9**, 2037–2046, DOI: 10.1039/d0tc05631f.

19 D. Gao, X. Bao, B. Lyu, Z. Chen, A. Zhang and J. Ma, Enhancing the stability of Cs3Bi2Br9 quantum dots for *anti*-counterfeiting applications in leather through polyacrylate coating, *J. Mater. Chem. C*, 2025, **13**, 7327–7335, DOI: 10.1039/d4tc04709e.

20 M. Fernández-Álvarez, S. Marín-Cortés, A. Moure and J. F. Fernández, Towards quantification of luminance values in photoluminescence and Raman spectroscopies by using a reference material, *J. Alloys Compd.*, 2025, **1015**, 178861, DOI: 10.1016/j.jallcom.2025.178861.

21 Y. C. Yiu and Z. Chu, A Multilevel Optical Anticounterfeiting System Based on Color Space-Correlated Raman Spectroscopy of Diamond, *Adv. Photonics Res.*, 2023, **4**, 2200281, DOI: 10.1002/adpr.202200281.

22 Z. Yang, X. Zhao, J. Liu, J. Wen, F. Zhang, X. Guo, K. Zhang, J. Zhang, A. Wang, R. Gao, Y. Wang and Y. Zhang, Designed Growth of AgNP Arrays for Anti-counterfeiting Based on Surface-Enhanced Raman Spectroscopy Signals, *ACS Appl. Mater. Interfaces*, 2022, **14**, 50024–50032, DOI: 10.1021/acsami.2c12124.

23 S. Dogruer Erkok, M. M. Kimani, A. Lanzarotta and B. McCord, Detecting fentanyl analogs in counterfeit pharmaceuticals by surface-enhanced Raman spectroscopy using handheld Raman spectrometers, *Forensic Sci. Int.*, 2026, **378**, 112679, DOI: 10.1016/j.forsciint.2025.112679.

24 M. Fernández-Álvarez, A. Moure, J. J. Reinosa, E. L. Diz and J. F. Fernández, New Protocol for Twinning of Raman Devices Toward a Raman Intensity Harmonization, *Appl. Spectrosc.*, 2024, **78**, 837–850, DOI: 10.1177/00037028241260377.

25 Q. Wang, M. Zhang, S. Chen, Q. Yu, R. Wang, J. Guo and X. Kong, Anti-counterfeiting labels with controllable and *anti*-interference coding information based on core–shell Ag@SiO2 nanomaterials for ink printing, *Spectrochim. Acta, Part A*, 2025, **325**, 125113, DOI: 10.1016/j.saa.2024.125113.

26 W. Wei, L. Wang, Q. Huang and T. Li, Controlled synthesis of biocompatible rGO@CD@Au nanocomposites for trace detection for doxorubicin by Raman imaging spectroscopy, *J. Alloys Compd.*, 2019, **783**, 37–43, DOI: 10.1016/j.jallcom.2018.12.285.

27 M. Fernández-Álvarez, A. Moure, P. Rabasco, E. Gómez, V. García-Juez and J. F. Fernández, Spectral harmonization of Raman data for reliable *anti*-counterfeiting analysis, *Microchem. J.*, 2025, **217**, 115010, DOI: 10.1016/j.microc.2025.115010.

28 A. Moure, J. F. Fernandez, V. Fuertes de la Llave, E. Enriquez and V. García Juez, WO2020152160A1, RAMAN MARKERS, 2020.

29 D. Yu, W. Zhu and A. G. Shen, Raman encoding for security labels: a review, *Nanoscale Adv.*, 2023, **5**, 6365–6381, DOI: 10.1039/d3na00707c.

30 M. A. Fikiet, D. Tuschel, V. V. Ermolenkov and I. K. Lednev, Clarifying Glass Luminescence at Near-Infrared Excitation, *Appl. Spectrosc.*, 2020, **74**, 187–192, DOI: 10.1177/0003702819879109.

31 C. Lenz, L. Nasdala, D. Talla, C. Hauzenberger, R. Seitz and U. Kolitsch, Laser-induced REE3+ photoluminescence of selected accessory minerals - An ''advantageous artefact'' in Raman spectroscopy, *Chem. Geol.*, 2015, **415**, 1–16, DOI: 10.1016/j.chemgeo.2015.09.001.

32 M. Fernández-Álvarez, P. Rabasco, G. Esther, V. García-Juez, J. F. Fernández and A. Moure, Design of glass-ceramic/diamond Raman markers for *anti*-counterfeiting applications, *Ceram. Int.*, 2026, DOI: 10.1016/j.ceramint.2026.04.326.

33 J. H. Hooijschuur, M. F. C. Verkaaik, G. R. Davies and F. Ariese, Raman spectroscopy for future planetary exploration: Photodegradation, self-absorption and quantification of carotenoids in microorganisms and mineral matrices, *J. Raman Spectrosc.*, 2015, **46**, 856–862, DOI: 10.1002/jrs.4647.

34 N. Kuhar, S. Sil, T. Verma and S. Umapathy, Challenges in application of Raman spectroscopy to biology and materials, *RSC Adv.*, 2018, **8**, 25888–25908, DOI: 10.1039/c8ra04491k.

35 S. Marín-Cortés, V. Fuertes, A. Serrano, J. López-Sánchez, M. Fernández-Álvarez, S. Román-Sánchez, M. París Ogáyar, D. Muñoz, M. J. Cabrera, J. F. Fernández and E. Enríquez, (Ca,Sr)(K,Na)AlSi3O8:Eu3+ photoluminescent pigment for traceability applications in ceramics, *J. Eur. Ceram. Soc.*, 2025, **45**, 117352, DOI: 10.1016/j.jeurceramsoc.2025.117352.

36 E. C. Trottier, S. Affrossman and R. A. Pethrick, Rheological studies of the cure of epoxy/polyester powder coatings containing titanium dioxide, *J. Coat. Technol. Res.*, 2012, **9**, 725–733, DOI: 10.1007/s11998-012-9417-7.

37 A. Sacco, L. Mandrile, L. L. Tay, N. Itoh, A. Raj, A. Moure, A. Del Campo, J. F. Fernandez, K. R. Paton, S. Wood, H. Kwon, T. Adel, A. R. Hight Walker, E. H. Martins Ferreira, R. Theissmann, T. Koch, A. M. Giovannozzi, C. Portesi and A. M. Rossi, Quantification of titanium dioxide (TiO2) anatase and rutile polymorphs in binary mixtures by Raman spectroscopy: an interlaboratory comparison, *Metrologia*, 2023, **60**(5), 055011, DOI: 10.1088/1681-7575/acf76d.

38 S. Marín-Cortés, M. Fernández-Álvarez, E. Enríquez and J. F. Fernández, Experimental characterisation data on aggregates from construction and demolition wastes for the assistance in sorting and recycling practices, *Constr. Build. Mater.*, 2024, **435**, 136798, DOI: 10.1016/j.conbuildmat.2024.136798.

 

39 S. Marín-Cortés, M. Fernández-Álvarez, A. Moure, J. F. Fernández and E. Enríquez, Chemometric-driven quantification of construction and demolition waste using Raman spectroscopy and SWIR: Enhancing sustainability in the ceramic sector, *Resour., Conserv. Recycl.*, 2023, **199**, 107259, DOI: 10.1016/J.RESCONREC.2023.107259.

40 K. J. R. Da Silva, W. Paschoal, E. A. Belo and S. G. C. Moreira, Phase Transition in all-trans-β-Carotene Crystal: Temperature-Dependent Raman Spectra, *J. Phys. Chem. A.*, 2015, **119**, 9778–9784, DOI: 10.1021/acs.jpca.5b04724.

41 I. Lorite, J. J. Romero and J. F. Fernandez, Study of the nanoparticle/microparticle powder systems by dry dispersion, *Ceram. Int.*, 2013, **39**, 1631–1637, DOI: 10.1016/j.ceramint.2012.08.005.

42 C. Medina-Gutiérrez, C. Frausto-Reyes, J. Medina-Valtierra, R. Jaimes-Reátegui, H. García-López and J. R. Molina-Contreras, Study of temperature effect in β-carotene of carrot by Raman spectroscopy, Fifth Symp. Opt. Ind. 6046, 2006, 60460Y, DOI: 10.1117/12.674466.

43 G. Knockaert, S. K. Pulissery, L. Lemmens, S. Van Buggenhout, M. Hendrickx and A. Van Loey, Isomerisation of carrot β-carotene in presence of oil during thermal and combined thermal/high pressure processing, *Food Chem.*, 2013, **138**, 1515–1520, DOI: 10.1016/j.foodchem.2012.10.080.

44 D. Martin, A. M. Amado, A. G. Gonzálvez, M. P. M. Marques, L. A. E. Batista De Carvalho and Á. G. Ureña, FTIR Spectroscopy and DFT Calculations to Probe the Kinetics of β-Carotene Thermal Degradation, *J. Phys. Chem. A*, 2019, **123**, 5266–5273, DOI: 10.1021/acs.jpca.9b02327.

45 Y. Koyama, I. Takatsuka, M. Nakata and M. Tasumi, Raman and infrared spectra of the all-trans, 7-cis, 9-cis, 13-cis and 15-cis isomers of β-carotene, *J. Raman Spectrosc.*, 1988, **19**, 37–49.

46 D. Dutta, A. Dutta, U. Raychaudhuri and R. Chakraborty, Rheological characteristics and thermal degradation kinetics of beta-carotene in pumpkin puree, *J. Food Eng.*, 2006, **76**, 538–546, DOI: 10.1016/j.jfoodeng.2005.05.056.

47 I. Mader, Beta-Carotene: Thermal Degradation, *Science*, 1964, **144**, 533–534.

48 Y. Huo, Z. Yang, T. Wilson and C. Jiang, Recent Progress in SERS-Based Anti-counterfeit Labels, *Adv. Mater. Interfaces*, 2022, **9**, 1–18, DOI: 10.1002/admi.202200201.